

# Particle Trapping in Axisymmetric Electron Holes

I H Hutchinson

Plasma Science and Fusion Center  
and Department of Nuclear Science and Engineering,  
Massachusetts Institute of Technology, Cambridge, MA 02139, USA.

## Abstract

Electron orbits are calculated in solitary two-dimensional axisymmetric electrostatic potential structures, typical of plasma electron holes, in order to establish the conditions for the particles to remain trapped. Analytic calculations of the evolution of the parallel energy caused by the perturbing radial electric field (breaking magnetic-moment invariance) are shown to agree well with full numerical orbit integration Poincaré plots. The predominant mechanism of detrapping is resonance between the gyro frequency in the parallel magnetic field and harmonics of the parallel bounce frequency. A region of phase-space adjacent to the trapped-passing boundary in parallel energy is generally stochastic because of island overlap of different harmonics, but except for very strong radial electric field perturbation, more deeply trapped orbits have well-defined islands and are permanently confined. A simple universal quantitative algorithm is given, and its results plotted as a function of magnetic field strength and hole radial scale-length, determining the phase space volume available to sustain the electron hole by depression of the permanently trapped distribution function.

## 1 Background

Electron holes are steady solitary electrostatic positive potential structures that sustain themselves by an electron density deficit arising from depressed phase-space density on trapped orbits [1–4]. They are frequently observed in one-dimensional non-linear simulations of plasma kinetic instabilities [4–8], and in observations of space plasmas [9–21]. The one-dimensional theory of these hole equilibria is well established, being a type of BGK mode [22]. However, in multiple dimensions, both the equilibrium and stability of these self-sustaining structures is far less well understood. Satellite observations show that electron holes are generally three-dimensional [23–26], oblate structures, more extended in the direction perpendicular to the ambient magnetic field, than parallel, but by an amount that varies with plasma and hole parameters. Also, analysis and simulation have shown that initially-one-dimensional holes are subject to instabilities [8, 27–37] that break them up in the transverse dimension, forming multidimensional remnants.

A significant magnetic field is known theoretically to be necessary for the existence of multidimensional electron hole equilibria in non-pathological background electron distributions [38–40]. When the field is strong enough that the gyro-radius ( $\rho$ ) is very small, the equilibrium becomes locally one-dimensional [41, 42], with minor corrections to Poisson’s equation to account for any transverse electric field divergence, but eventually negligible influence on the particle orbits. At the other extreme, the magnetic field cannot be so weak as to make the gyro-radius large compared with the hole’s transverse dimensions, otherwise it provides little transverse confinement. But there is a big parameter range between these two limits, in which virtually no theory beyond order of magnitude heuristics has been completed. A high proportion of observed electron holes have equilibrium parameters lying in this unexplained region, see for example [23–25].

This article presents a first step to carry out rigorous analysis of multidimensional electron hole equilibria. It adopts a model potential that is axisymmetric (independent of the angle  $\theta$  in a cylindrical coordinate system) which is a representative subset of three-dimensional holes. The electron orbits in this equilibrium are analysed and calculated numerically, to discover which regions of phase space are permanently trapped; and, in contrast, the regions that initially possess small enough parallel kinetic energy to be trapped by the parallel electric field, but evolve soon to become untrapped, by the transfer of energy from perpendicular gyration. By time reversal symmetry, equivalent orbits (in equal numbers) experience evolution of parallel energy from passing to become trapped. There thus arises a large effective parallel energy diffusion across the trapped/passing boundary. These detrapping/trapping orbits cannot sustain depressed electron phase-space density, and so cannot contribute to maintaining the hole’s positive potential, because the important detrapping occurs usually on a short timescale of a moderate number of bounces, i.e. approximately of plasma periods.

The present work does not solve the (still unsolved) full problem of finding a self-consistent equilibrium in which only the velocity distribution function on the permanently trapped orbits is allowed to differ from the background distribution. But it does give limits on what fully self consistent solutions can exist, and indicates what their distribution functions might look like.

## 2 Orbits in axisymmetric electron holes

We consider the orbits of electrons in a potential  $\phi(r, z)$  that is axisymmetric about the coordinate  $z$ . This is a 2D problem, meaning there is just one ignorable coordinate  $\theta$ . A 2D cartesian geometry in which one cartesian coordinate is ignorable would give essentially the same result, and can be considered to be the limit in which the radius  $r$  is large.

In the 1D case where  $\phi$  depends only on  $z$ , there are two exact constants of the motion which are the total energy  $W$  and the magnetic moment, which in the present uniform magnetic field can be taken as the perpendicular kinetic energy  $W_{\perp}$ . The perpendicular motion is then entirely decoupled from the parallel and can be ignored. However, when  $\phi$  varies with radius  $r$ , and a transverse electric field  $E_r$  exists, the  $W_{\perp}$  (magnetic moment) invariance is broken, and the only strict invariant in addition to  $W$  is the canonical angular momentum about the  $z$ -axis:  $p_{\theta} = r(v_{\theta} - \Omega r/2)$ , where  $\Omega$  is the gyro-frequency. The effect of  $p_{\theta}$  conservation is mostly to restrict the range of variation of the orbit’s radius to what in the

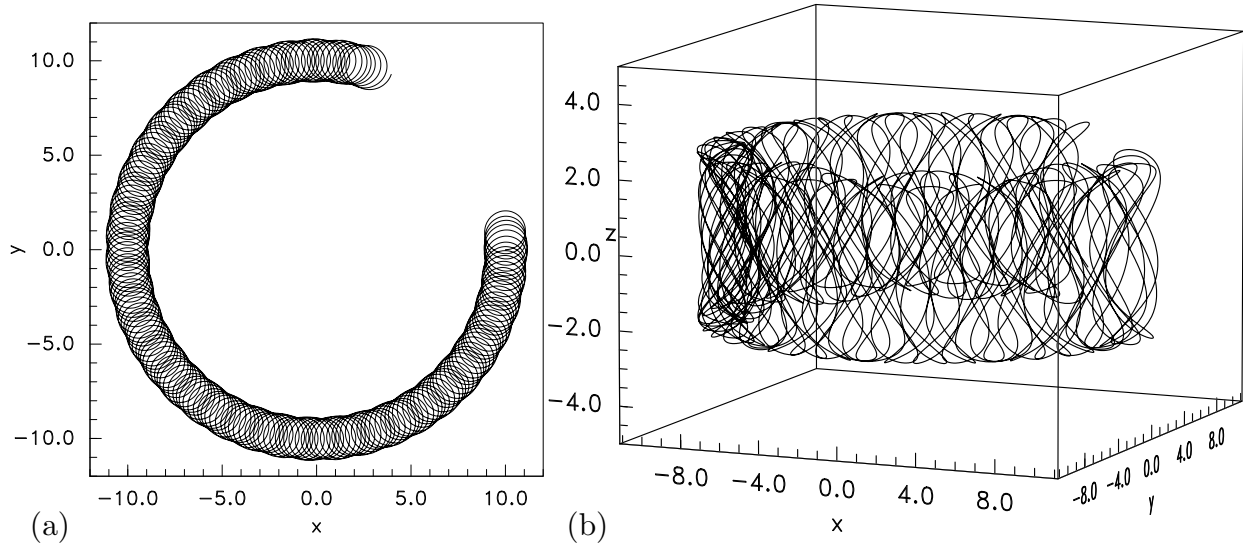


Figure 1: Example of a trapped electron orbit in a model electron-hole potential  $\phi = \psi \exp([r_0 - r]/L_\perp) \text{sech}^4(z/4)$ , starting at  $x = r_0$ ,  $y = 0$ ,  $z = 0$ ,  $v_x = 1$ ,  $v_y = 0$ ,  $v_z = 1$ . Viewed (a) in the transverse  $x, y$  plane, and (b) in three-dimensions showing the bouncing parallel to the magnetic field ( $z$ ) direction. (Parameters:  $\psi = 1$ ,  $\Omega = 0.9$ ,  $r_0 = 10$ ,  $1/L_\perp = 0.05$ .)

probe literature are called “magnetic bottles” (e.g. [43]). At radii greater than approximately the gyro-radius  $\rho = v_\perp/\Omega$ , conservation of  $p_\theta$  contributes little to parallel particle dynamics, serving mostly to localize the orbit in radial position, within approximately one gyro-radius. Fig. 1 illustrates the kind of orbit that results.

For an electron hole to sustain itself requires a substantial fraction of the particle orbits to be trapped. These orbits can then permanently possess a phase-space density ( $f$ ) less than those of untrapped orbits. Because in a collisionless plasma  $f$  is constant along orbits, the *untrapped* orbits have phase-space density corresponding to their distribution function at infinity; whereas the permanently *trapped* orbits have  $f$  determined by initial conditions: the hole formation processes etc. The key question concerning the existence of a steady solitary electron hole equilibrium is whether there are enough permanently trapped orbits to provide a negative electron density perturbation that can sustain the potential structure self-consistently.

Isotropic multidimensional electron hole equilibria do not exist because the trapped phase space is then only orbits which have  $W < 0$ , and in  $d$ -dimensions this volume  $\propto \phi^{d/2}$  is insufficient when  $d > 1$  [38–40]. Particle in cell simulation and drift-orbit analysis show that there exist axisymmetric 2D equilibria, with anisotropic  $f(\mathbf{v})$ , when the magnetic field is strong enough that the gyro-radius ( $\rho$ ) is negligibly small. Essentially this existence arises because of the adiabatic invariance of  $W_\perp$  and hence  $W_\parallel = W - W_\perp$  in the limit of small  $\rho$ . The trapped phase-space volume is then larger ( $\propto \phi^{1/2}$ ), requiring only  $W_\parallel < 0$  and extending to large positive  $W_\perp$ . For the intermediate case, where  $\rho$  is finite, yet transverse  $\phi$ -variation exists, the challenge is this. Given that, for finite magnetic field strength, energy can be exchanged during the orbit between  $W_\parallel$  and  $W_\perp$ , can one quantify whether and to

what extent the amount exchanged is limited, and an orbit remains trapped in the  $z$ -direction ( $W_{\parallel} < 0$ ) even if it has so large a  $W_{\perp}$  that  $W > 0$ ? An earlier attempt on this problem used a more complicated treatment based on an “approximate invariant” [44] but was not carried through to a full result. The present paper overcomes the challenge.

Although the calculation will remain as general as possible, we shall have in mind equipotentials that are oblate: varying faster in the parallel ( $z$ ) direction than in the transverse ( $r$ ) direction. For convenience we assume that the  $z$ -dependence of  $E_r = -\nabla_{\perp}\phi$  is the same as that of  $\phi$ , as would be the case if  $\phi$  is of separable form  $\phi_r(r)\phi_z(z)$ .

We work in units where time is measured in inverse plasma frequencies ( $\omega_p = \sqrt{n_e e^2 / m_e \epsilon_0}$ ), length in Debye lengths ( $\lambda_{De} = \sqrt{\epsilon_0 T_e / e^2 n_e}$ ), and energies (and potential) in electron temperatures ( $T_e$ ). Thus if primes denote dimensioned parameters, and unprimed the normalized quantities,  $t = \omega_p' t'$ ,  $\mathbf{x} = \mathbf{x}' / \lambda_{De}'$ , and energy  $W = W' / T_e$ . The parameters  $T_e$  and  $n_e$  are the temperature and density of the unperturbed electron distribution far from the hole. In these units the electron mass is eliminated from the equations, and the electron charge is  $q_e = -1$ , so the total energy of an electron can be written  $W = \frac{1}{2}v^2 - \phi$ . We shall refer to the parallel energy as  $W_{\parallel} = \frac{1}{2}v_{\parallel}^2 - \phi$  and perpendicular as  $W_{\perp} = \frac{1}{2}v_{\perp}^2 = \frac{1}{2}(v_r^2 + v_{\theta}^2)$ . The magnetic field strength is represented by the (normalized) cyclotron frequency  $\Omega (= \Omega' / \omega_p')$ . The equation of an electron orbit is then

$$\frac{d\mathbf{v}}{dt} = \nabla\phi - \mathbf{v} \times \Omega\hat{\mathbf{z}}. \quad (1)$$

We treat changes in magnetic moment as slow. This is justified if the transverse electric field (arising from transverse non-uniformity of  $\phi$ ) is small in the sense that  $E_r/\phi \ll 1/\rho$ , which may also be written  $L_{\perp} \gg \rho$ , where  $L_{\perp} \equiv \phi/E_r = \phi/|\partial\phi/\partial r|$  is the transverse length scale of potential variation. Starting from the drift limit (which is essentially  $\rho/L_{\perp} \rightarrow 0$ ), we recognize that the orbit’s gyrocenter moves freely along  $z$  under the influence of the parallel electric field, and simultaneously rotates azimuthally in  $\theta$  under the (time-varying) influence of  $\mathbf{E}_r \times \mathbf{B}/B^2$ . Trapped orbits (our main focus) bounce in  $z$  and experience an effectively periodic  $E_r$  as a consequence. The mean value of  $E_r$  over a period determines the average azimuthal rotation. The varying component of  $E_r$  is the perturbation responsible for the transfer between perpendicular and parallel energy. To first order, the fractional transfer of energy in a bounce period is small. Then during a single period,  $z(t)$  can be approximated as being given by parallel motion with fixed  $W_{\parallel}$ , which is simply the 1D orbit problem. Moreover  $E_r(t) = E_r(r, z(t)) = -\partial\phi(r, z(t))/\partial r$  can be approximated as being at fixed radius  $r$  (again provided  $\rho$  is small enough relative to  $L_{\perp}$ ). The instantaneous energy transfer rate (recalling that  $W = W_{\parallel} + W_{\perp}$  is exactly conserved) is simply the rate of doing work on the electron by  $E_r$ , namely

$$\frac{dW_{\parallel}}{dt} = -\frac{dW_{\perp}}{dt} = -E_r(t)v_r(t). \quad (2)$$

The important velocity component in this equation arises from the gyro motion of the electron,  $v_r = v_{\perp} \cos(\Omega t)$ . When this equation is integrated over many bounces and gyro-periods, large excursions in  $W_{\parallel}$  will occur if there is a resonance between the gyro frequency and a harmonic of the bounce frequency  $\omega_b$ . These are the orbits that are liable to lead to detraping, because the energy transfer is consistently unidirectional (between  $W_{\perp}$  and  $W_{\parallel}$ ) over many bounce periods.

Fig. 2 illustrates an orbit (red) that quickly becomes detrapped and a permanently trapped orbit (blue), all as a function of parallel position. The top frame shows the track

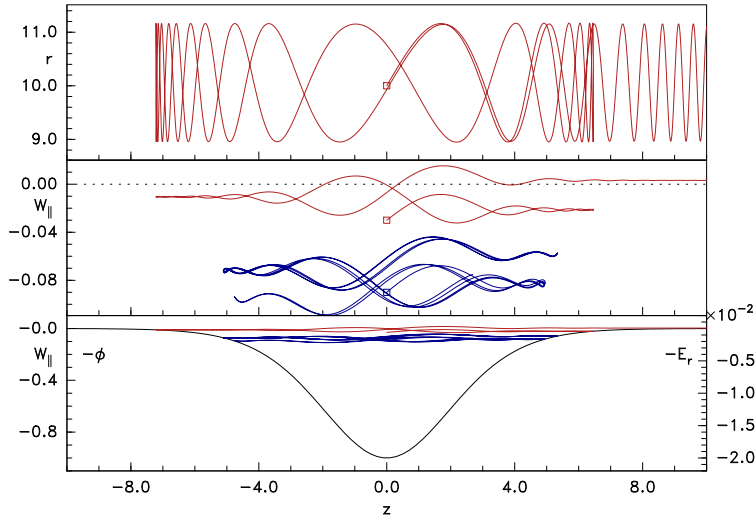


Figure 2: Example of detrapped and permanently trapped orbits. Parameters  $\psi = 1$ ,  $\Omega = 1.29$ ,  $W = 1$ ,  $E_r = 0.02$ , and initial  $W_{\parallel} = -0.03$ (red),  $-0.09$ (blue) marked with a square.

$(r(t), z(t))$  in the  $r$ - $z$  plane combining gyro-motion and parallel reflections (the blue orbit is omitted in this frame for clarity, but has the same radial excursion). The middle and bottom frames show instead the parallel energy  $W_{\parallel}(z, t)$  and the bottom shows  $-\phi(z)$  and (read on the right scale)  $E_r(z)$ . The detrapped orbit has two  $z$ -reflections before acquiring  $W_{\parallel} > 0$  at the right-hand hole extremity and leaving the hole, becoming untrapped. The trapped orbit has many more bounces with excursions in  $W_{\parallel}$  never reaching zero because it lies somewhat deeper in the potential well. If near-resonant orbits do not lead *directly* to detrapping, by raising  $W_{\parallel}$  above zero, like the red orbit here, then they generally take the form of “islands” in the coordinate space  $W_{\parallel}$  versus relative phase angle (to be explained more fully in a moment). The result then is that the orbits remain trapped. The blue orbit and essentially all in this hole with even more negative initial  $W_{\parallel}$  are of this type.

Since there are multiple resonances arising from the harmonics of  $\omega_b$ , the orbits can become stochastic and the islands broken up. Very generally, stochasticity begins in Hamiltonian systems approximately when there is overlap between the separatrices of adjacent islands [45, 46]. Indeed, this principle is called the Chirikov criterion in recognition of its discoverer who studied resonances between gyro motion and bounces along the magnetic field in magnetic traps [47]: a close analog of our current concern. If an orbit is stochastic, it is generally *not* permanently trapped, and in principle cannot contribute to hole sustainment. Our analytic determination of the orbit trajectories in  $W_{\parallel}$  disregards the radial variation of  $\phi$  and  $E_r$ : an appropriate approximation for small gyroradius (but the full orbit integration, also presented, does not).

### 3 Islands in energy

When discussing resonant perturbation islands in a Hamiltonian system, one generally requires an angle-like coordinate that amounts to the phase difference between the Hamiltonian orbit and the perturbation. In the magnetized electron hole with (presumed) uniform  $\Omega$ , the phase difference we require is between the gyro motion (of  $v_\perp$  and hence phase of  $v_r$ ) and a perturbing electric field which we will take as the Fourier component  $E_n$  at some harmonic  $n$  of the slowly varying bounce frequency:  $\omega_n = n\omega_b$ . The Fourier component has a fixed phase with respect to the  $z$  motion, which we will take as zero when  $z = 0$ . But because  $\omega_b$  varies with  $W_\parallel$ , the bounce phase has a variable rate of change with respect to the gyrophase, whose phase we have taken as zero when  $v_r = v_\perp$ . We shall write the phase difference between bounce and gyromotion as  $\xi$ , so that

$$\frac{d\xi}{dt} = \omega_n - \Omega, \quad (3)$$

and seek the locus of orbit motion in the plane  $\xi, W_\parallel$ . Orbits will then have

$$\begin{aligned} \frac{dW_\parallel}{dt} &= -E_n v_\perp \cos(\omega_n t) \cos(\Omega t) \\ &= -E_n v_\perp \frac{1}{2} [\cos(\omega_n - \Omega)t + \cos(\omega_n + \Omega)t] \\ &\simeq -\frac{1}{2} E_n v_\perp \cos \xi, \end{aligned} \quad (4)$$

and we have dropped the term  $\cos(\omega_n + \Omega)t$ , because it is a fast oscillation, compared with the presumed slow evolution of  $\xi = (\omega - \Omega)t$ . We shall mention it later.

Let us suppose for initial illustrative purposes that the variation of  $\omega_n$  with  $W_\parallel$  can be approximated linearly as

$$\frac{d\xi}{dt} = \omega_n - \Omega = \frac{d\omega_n}{dW_\parallel} (W_\parallel - W_{\parallel R}) = \frac{d\omega_n}{dW_\parallel} \Delta W_\parallel, \quad (5)$$

where  $W_{\parallel R}$  is the value of  $W_\parallel$  at which exact resonance occurs ( $\omega_n = \Omega$ ), and that we can take  $E_n$  and  $\frac{d\omega_n}{dW_\parallel}$  to be independent of  $W_\parallel$ . Then eq. (2) becomes

$$\frac{d\omega_n}{dW_\parallel} \Delta W_\parallel \frac{dW_\parallel}{d\xi} = \frac{d\omega_n}{dW_\parallel} \frac{d\Delta W_\parallel^2}{2d\xi} = -E_n v_\perp \frac{1}{2} \cos \xi. \quad (6)$$

This expression can be integrated as

$$\frac{d\omega_n}{dW_\parallel} \Delta W_\parallel^2 = -E_n v_\perp \sin \xi + C. \quad (7)$$

This is the island locus, and different values of the integration constant,  $C$ , give rise to different trajectories, effectively different starting  $W_\parallel$ s. The island's separatrix corresponds to  $C = E_n v_\perp$ . The x-point (if  $\frac{dW_\parallel}{d\omega_b}$  is negative) is at  $\xi = -\pi/2$  and the (maximum) half-width of the separatrix (at  $\xi = \pi/2$ ) is then

$$|\Delta W_\parallel| = \sqrt{2E_n v_\perp \left| \frac{dW_\parallel}{d\omega_n} \right|}. \quad (8)$$

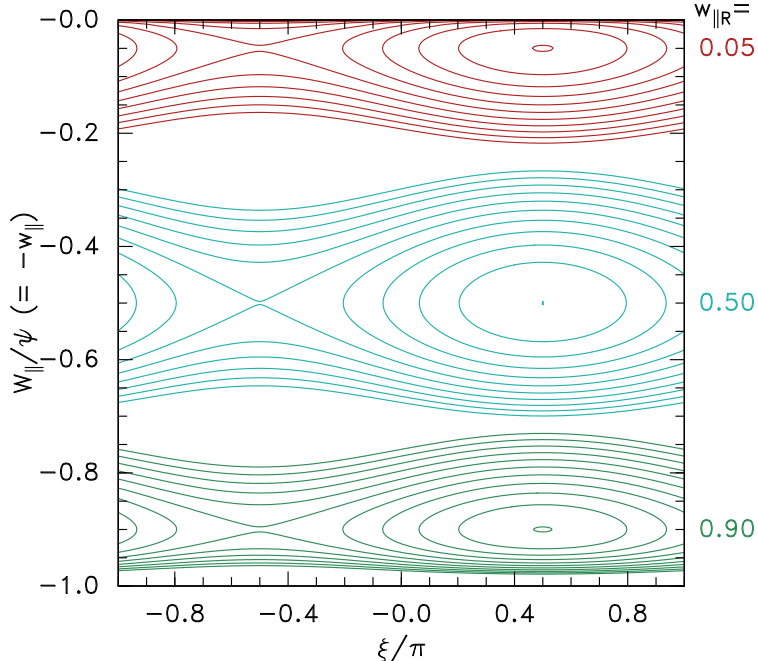


Figure 3: Example energy trajectories for different magnetic field strengths, all for the lowest harmonic  $n = 2$ .

The island center is at  $\xi = \pi/2$ ,  $C = -E_n v_\perp \frac{dW_\parallel}{d\omega_n}$ .

The result is most usefully plotted as contours of the constant  $C$ , in the  $\xi$ - $W_\parallel$  plane, which trace the trajectories of the orbits. Figure 3 shows examples from a more elaborate calculation (and will be explained more fully in section 5.1), but the blue contours in it, centered on  $W_\parallel/\psi = -0.5$ , have approximately the shape obtained with the simple approximations used in this introductory section.

## 4 The electric field harmonics

We must now obtain expressions for  $\omega_b$  and  $E_n$  as a function of  $W_\parallel$  for a model electron hole. These depend upon the  $z$ -profile of the potential, which will be taken as

$$\phi(r, z) = \psi(r) \text{sech}^4(z/4). \quad (9)$$

This  $z$ -dependence is what is obtained for 1-D shallow holes whose trapped distribution is a Maxwellian of negative temperature [48]. More importantly, it falls off at large distances  $\propto \exp(-z)$ , which is *required* for essentially any 1-D Debye shielded potential (at small hole velocity) that does not have infinite velocity distribution derivative at  $W_\parallel = 0$  [4]. Therefore the results we obtain from this model potential will apply to shallow trapped orbits for a wide range of acceptable potential profiles (which is not the case for Gaussian shaped potentials, often used.) We approximate the orbit, for the purpose of determining the  $z$ -motion, as occurring at fixed  $r$  (because of  $p_\theta$  conservation), so it is effectively a 1-D problem in space.

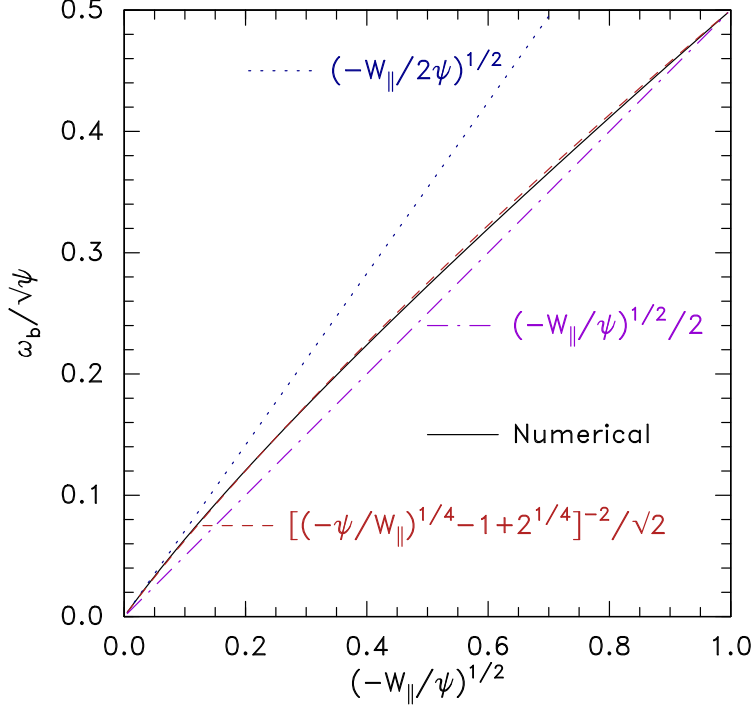


Figure 4: The energy dependence of bounce frequency  $\omega_b$  for trapped 1-D motion in a potential energy well  $-\psi \operatorname{sech}^4(z/4)$ . Numerical integration gives the solid line, and several limits and approximations are shown.

## 4.1 Bounce Frequency

It has been shown recently [37] that for shallow-trapping ( $-W_{\parallel} \ll \psi$ ) the (1D) bounce frequency is  $\omega_b \simeq \sqrt{-W_{\parallel}/2}$  in this potential. Deeply trapped orbits ( $W_{\parallel} + \psi \ll \psi$ ) have bounce frequency in the approximately parabolic bottom of the potential energy well  $\omega_b = \sqrt{\psi}/2$ . This expression is exact for the  $\operatorname{sech}^4$  profile chosen, but the potential shape at the peak can (unlike the hole wings) be different, so this is a choice of a particular shape of hole. It has been found by numerical orbit integration as shown in Fig. 4 that an interpolation of the universal form

$$\omega_b/\sqrt{\psi} = [(-W_{\parallel}/\psi)^{-1/4} - 1 + 2^{1/4}]^{-2}/\sqrt{2}, \quad (10)$$

represents the dependence over the entire trapped energy range extremely well, within approximately the thickness of the line. The inverse of this expression is

$$-W_{\parallel}/\psi = [(2\omega_b^2/\psi)^{-1/4} + 1 - 2^{1/4}]^{-4}. \quad (11)$$

The shallow  $W_{\parallel} \rightarrow 0$  limit line  $\omega_b = \sqrt{-W_{\parallel}/2}$  is indicated by the dotted line. For approximate analytic purposes (to avoid the eventual necessity to evaluate hypergeometric functions) it is adequate to adopt a more approximate form

$$\omega_b/\sqrt{\psi} = (-W_{\parallel}/\psi)^{1/2}/2, \quad (12)$$

the dot-dash line with constant slope of 1/2 in Fig. 4.



Now we must relate the bounce motion to the time harmonics of  $E_r$ . First, observe that for a mirror symmetric potential such as eq. (9) the period of the variation of  $E_r = -\partial\phi/\partial r$  with  $z$  at constant  $r$  is actually  $\pi/\omega_b$ , and so only even harmonics  $n\omega_b$  are non-zero. The harmonics  $n > 2$  arise from the anharmonic motion and the resulting deviations of  $E_r(t)$  from a pure sinusoid.

Let us introduce convenient energy parameter notation involving positive values normalized to  $\psi$ , and (for future use) cyclotron frequency to  $\sqrt{\psi}$  as

$$w_{\parallel} \equiv -W_{\parallel}/\psi, \quad w \equiv W/\psi, \quad b \equiv \Omega/\sqrt{\psi}; \quad (13)$$

so trapped orbits have  $w_{\parallel}$  running from 0 to 1, and the orbits that can become untrapped have  $w > 0$ . For a given magnetic field value  $b$ , and harmonic number  $n$ , the resonance condition is  $n\omega_b/\sqrt{\psi} = b$ , which gives a resonant parallel energy

$$w_{\parallel R} = [(2b^2/n^2)^{-1/4} + 1 - 2^{1/4}]^{-4} \quad (14)$$

corresponding to eq. (11).

## 4.2 Shallow trapped orbits

For shallow-trapped orbits, the  $E_r(t)$  has the form of a train of relatively narrow impulses of width  $\sim \tau_t$  and period  $\pi/\omega_b$ , which peak briefly as the orbit passes rapidly through  $z \simeq 0$ . The orbit spends most of its time near the extrema of the  $z$ , where the parallel electric field is very small; and this dwell duration determines the period [37]. The total impulse in a single passage can be written  $A = \int E_r dt$ , and its duration is approximately the potential width divided by the peak speed [ $\tau_t \simeq 8/\sqrt{2(\psi + w_{\parallel})}$ ]. When  $w_{\parallel}/\psi \rightarrow 0$ , the integral  $\int E_r(z) dt = \int E_{r0} \operatorname{sech}^4(z/4) dz/v_{\parallel}(z)$  can be performed exactly and yields  $A = 8E_{r0}/\sqrt{2\psi}$ . The Fourier decomposition of  $E_r(t)$  then gives the following Fourier mode amplitudes  $E_n$ , for even  $n$  when  $\tau_t \lesssim \pi/\omega_n$  (i.e.  $\sqrt{-W_{\parallel}/\psi} = \sqrt{w_{\parallel}} \lesssim \pi/4n$ ):

$$E_n = A \frac{2\omega_b}{\pi} \simeq E_{r0} \frac{8}{\pi} \sqrt{-W_{\parallel}/\psi} = E_{r0} \frac{8}{\pi} \sqrt{w_{\parallel}}. \quad (15)$$

We will refer to this as the impulse limit.

## 4.3 High Bounce Harmonics

An alternative perspective of the impulse limit is to note that each impulse gives an energy change  $\delta w_{\parallel} = -Av_r = -Av_{\perp} \cos \xi$ , every  $\delta t = \pi/\omega_b$ . If  $\delta \xi$  and  $\delta w_{\parallel}$  during a single passage through  $z = 0$  are small, we may approximate the effect as an average energy rate of change

$$\frac{dw_{\parallel}}{dt} = \frac{\delta w_{\parallel}}{\delta t} = -\frac{Av_{\perp}\omega_b}{\pi} \cos \xi, \quad (16)$$

in agreement with eqs. (15), and (4).

However, if  $\Omega \gg \omega_b$ , so that only high harmonics of  $\omega_b$  are resonant, the continuum limit is inappropriate. Moreover, it will always be the case that  $\Omega \gg \omega_b$  near the trapping boundary,  $w_{\parallel} \rightarrow 0$ , because  $\omega_b \rightarrow 0$  there.

When there are many cyclotron periods during one bounce period, but the cyclotron period is still long compared with the impulse duration,  $\tau_t$  (which does not itself become significantly longer as  $w_{\parallel} \rightarrow 0$ ), the cyclotron phase ( $\xi$ ) at which each succeeding impulse occurs becomes effectively random relative to the previous impulse. So, rather than a systematic continuous flight in the  $(\xi, w_{\parallel})$  space, the evolution consists of steps of virtually random amplitude  $\delta w_{\parallel}$  cosine-distributed between  $\pm Av_{\perp}$ . This represents an effective *diffusion* in  $w_{\parallel}$  with a diffusion coefficient  $\sim (Av_{\perp})^2 \omega_b / \pi$ . Moreover, for passing particles, which are addressed in a recent paper [49] concerning the scattering of passing particles by successive encounters with different electron holes, one similarly arrives at velocity space diffusion. The diffusion connects the trapped orbit region  $w_{\parallel} < 0$  with the untrapped region  $w_{\parallel} > 0$  across the nominal phase-space separatrix  $w_{\parallel} = 0$ , with the result that the distribution function in this region has only limited gradient  $|df/dw_{\parallel}|$ , and a value approximately equal to the external distribution  $f_{\infty}$  at  $v_{\parallel} = 0$  (in the frame of reference of the hole). This is one crucial constraint on possible electron-hole equilibria.

#### 4.4 Deeply trapped orbits

Orbits that are deeply trapped, having  $-W_{\parallel}/\psi$  a significant fraction of unity, are not accurately described by the impulse approximation of the previous section. Instead of being strongly anharmonic, the  $\phi(z)$  is approximately parabolic for them, and their orbit's  $z$ -position varies approximately sinusoidally in time. In the limit  $w_{\parallel} \rightarrow 1$ , only the lowest Fourier mode,  $n = 2$  is important and the higher harmonics become negligible. Moreover,  $E_r$  variation depends on the orbit's  $z$ -excursion size; so even for the lowest relevant harmonic  $\omega_n = 2\omega_b$ , the electric field Fourier amplitude  $E_n = E_2$  can become small.

The Taylor expansion of the potential  $\phi(z) = \psi \operatorname{sech}^4(z/4)$  about  $z = 0$  is  $\phi(z) \simeq \psi[1 - z^2/8 + 7z^4/768 + O(z^6)]$ , which leads to the sinusoidal bounce frequency  $\omega_b = \sqrt{\psi}/2$  when  $z^4$  and higher terms are dropped. The presumed similar radial electric field likewise has  $E_r(z) \simeq E_{r0}(1 - z^2/8)$ , of which the time varying part is only the second term. For given parallel energy,  $w_{\parallel}$  the amplitude  $z_{\max}$  of the  $z$ -oscillation satisfies  $z_{\max}^2/8 = (1 - w_{\parallel})$ , and  $E_r(t) = E_{r0}[1 - z_{\max}^2 \sin^2(\omega_b t)/8] = E_{r0}[(1 - z_{\max}^2/16) + z_{\max}^2 \cos(2\omega_b t)/16]$  then yields

$$E_2 = z_{\max}^2 E_{r0}/16 = E_{r0}(1 - w_{\parallel})/2. \quad (17)$$

This dependence on  $(1 - w_{\parallel})$  replaces the  $\sqrt{-w_{\parallel}}$  dependence of eq. (15).

#### 4.5 Interpolated $E_n$ expression

It is helpful to have an approximate analytic interpolation for the Fourier harmonics  $E_n$  that spans the entire range  $0 < w_{\parallel} < 1$ . Observe that  $1 - w_{\parallel} = (1 - \sqrt{w_{\parallel}})(1 + \sqrt{w_{\parallel}})$ ; so an alternative expression to eq. (17), which is equally valid in the limit  $w_{\parallel} \rightarrow 1$ , is  $E_2 = E_{r0}(1 - \sqrt{w_{\parallel}})$ . Realize also that the higher harmonics,  $n = 4, 6, \dots$ , arise from correspondingly higher order terms in the Taylor expansion of  $\phi(z)$ , and that therefore, as  $w_{\parallel} \rightarrow 1$ ,  $E_n$  will become proportional to correspondingly higher powers:  $(1 - \sqrt{w_{\parallel}})^{n/2}$ .

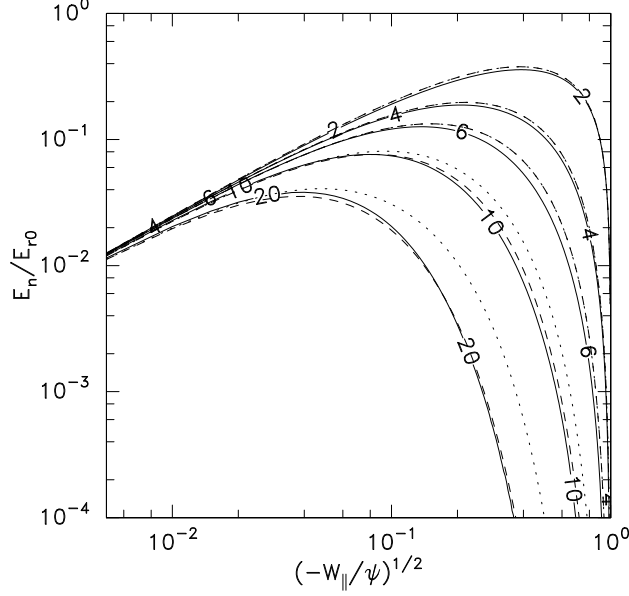


Figure 5: Comparison between numerically integrated Fourier coefficients for a  $\text{sech}^4(z/4)$  potential variation (solid lines) and the interpolation eq. (18) with  $m = n/2$  (dotted) or using eq. (19) (dashed lines), for different harmonic number (line labels).

Consider then the following proposed interpolation between the two limits of  $w_{\parallel}$ :

$$E_n = E_{r0} \left[ \frac{n/2}{(1 - \sqrt{w_{\parallel}})^m} + \frac{\pi}{8} \frac{1}{\sqrt{w_{\parallel}}} \right]^{-1}, \quad (18)$$

where for most purposes  $m = n/2$ . The first term predominates as  $w_{\parallel} \rightarrow 1$ , and the second as  $w_{\parallel} \rightarrow 0$ . In their respective limits, these two terms give the correct values for  $E_2$ , in agreement with eqs. 15 and 17. In the  $w_{\parallel} \rightarrow 1$  limit, the higher harmonics have appropriate scaling with  $1 - \sqrt{w_{\parallel}}$ . Their numerator  $n/2$  has not been derived; and, more crucially, neither has the inverse form of the interpolation. Nevertheless, a comparison between this expression and numerical calculation of the Fourier harmonics, shows quite good agreement, as can be seen in Fig. 5. This agreement is sufficient for many purposes, but some moderate discrepancies remain especially at high  $n$ . They are significantly reduced if an ad hoc adjustment is made by substituting

$$m = \text{nint}(n/2 + \max(n/2 - 3.3, 0) * 0.75) \quad (19)$$

(instead of  $m = n/2$ ) into eq. (18). The adjustment benefits from retaining convenient integrability.

## 5 Solving the $w_{\parallel}$ trajectories

### 5.1 Analytic calculation

Using the approximate expression (12) for  $\omega_b$  giving  $\omega_n = (n/2)\sqrt{\psi w_{\parallel}}$ , the energy trajectory equation (4) ignoring the fast  $\omega_n + \Omega$  term becomes

$$\begin{aligned} \frac{dw_{\parallel}}{dt} &= (\omega_n - \Omega) \frac{dw_{\parallel}}{d\xi} = \frac{n\sqrt{\psi}}{2} (\sqrt{w_{\parallel}} - \sqrt{w_{\parallel R}}) \frac{dw_{\parallel}}{d\xi} \\ &= \frac{1}{2} (E_n/\psi) v_{\perp} \cos \xi, \end{aligned} \quad (20)$$

where  $w_{\parallel R}$  is the resonant parallel energy at which  $\omega_n = \Omega$ . Substituting the interpolation for  $E_n$  from eq. (18), and  $v_{\perp} = \sqrt{2(w + w_{\parallel})\psi}$ , it can be written

$$\begin{aligned} n \frac{\sqrt{w_{\parallel}} - \sqrt{w_{\parallel R}}}{\sqrt{2}\sqrt{w + w_{\parallel}}} \left[ \frac{n/2}{(1 - \sqrt{w_{\parallel}})^m} + \frac{\pi}{8} \frac{1}{\sqrt{w_{\parallel}}} \right] \frac{dw_{\parallel}}{d\xi} \\ = (E_{r0}/\psi) \cos \xi. \end{aligned} \quad (21)$$

This equation can be integrated analytically in terms of elementary functions to obtain

$$F_n(w_{\parallel}, w, w_{\parallel R}) - (E_{r0}/\psi) \sin \xi = \text{const.}, \quad (22)$$

where for each  $n = 2, 4, 6, \dots$ ,  $F_n$  is a fairly complicated algebraic expression detailed in the appendix. For chosen total energy, magnetic field strength, and perturbing field (i.e.  $w$ ,  $w_{\parallel R}$ , and  $E_{r0}/\psi$ ) the trajectories can most easily be plotted as contours of the left hand side expression,  $F_n - (E_{r0}/\psi) \sin \xi$ , in the plane  $(\xi, w_{\parallel})$ . In these calculations it improves accuracy to use the more accurate equation (14) for  $w_{\parallel R}$  in terms of  $b$ , in  $F_n$ ; and we adopt this practice forthwith, ignoring the minor inconsistency.

In Fig. 3 are shown examples of the energy trajectories for  $w = 1$ ,  $E_r/\psi = 0.01$ ,  $\psi = 1$ , and three values of the magnetic field strength, and hence of the resonance energy  $w_{\parallel R}$  for the lowest harmonic  $n = 2$ . The perturbing field is quite strong and we can see that the trajectories near the top or bottom of the potential energy well (i.e. near to  $-w_{\parallel} = 0$  or  $-1$ ) are compressed asymmetrically at those limits because of the form of  $F_n$ . For an energy away from those limits, the contours are approximately symmetric about the resonant energy. If the magnetic field strength is big enough that  $\Omega^2/\psi > 1$ , then this  $n = 2$  resonance does not exist.

Fig. 6(a), instead shows trajectories for fixed magnetic field, and hence fixed  $n = 2$  resonance frequency, ( $b = \Omega/\sqrt{\psi} = \sqrt{0.8}$ ,  $E_{r0}/\psi = 0.005$ ), but for harmonic numbers  $n = 2, 4, 6, 8, \dots$ . The resonance energy is  $w_{\parallel R} = [(2b^2/n^2)^{-1/4} + 1 - 2^{1/4}]^{-4}$ . The higher harmonics bunch together near the top of the potential energy well, corresponding to low bounce frequency. And in fact the  $n = 6$  and  $n = 8$ , islands overlap: indicating that this region of energy has stochastic orbits and so the orbits there are not permanently trapped. Lower in the well, no overlap occurs with the  $n = 2$  island; so orbits there are permanently trapped.

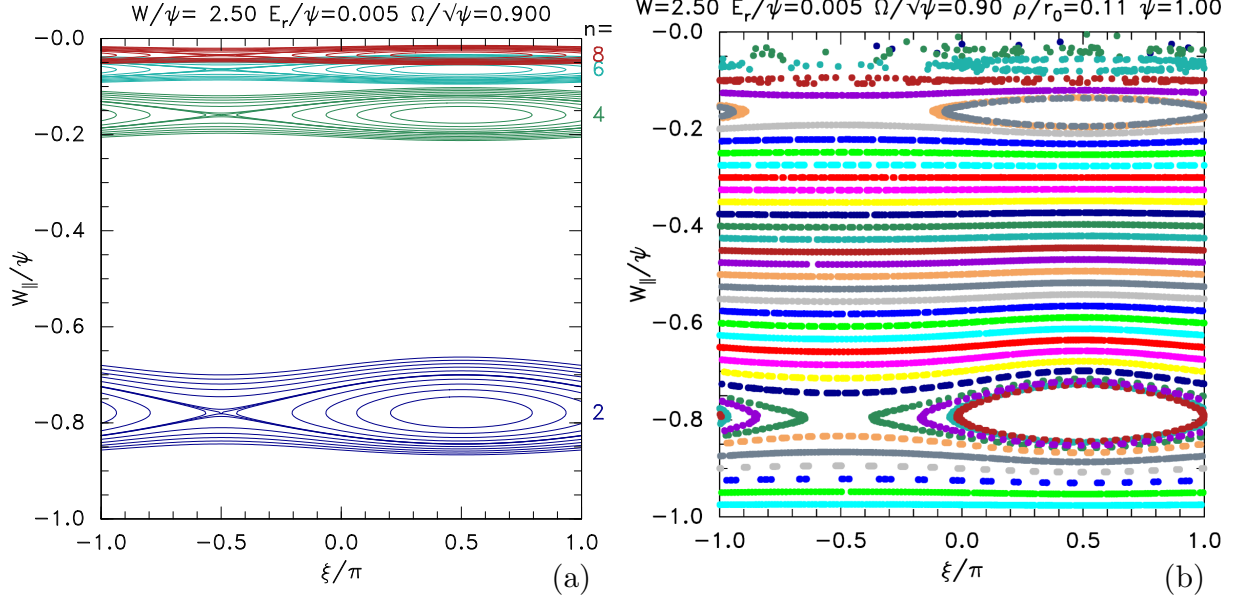


Figure 6: (a) Example analytic energy trajectories for different harmonics ( $n$ ), and fixed magnetic field strength. (b) Poincaré plot of the corresponding numerically integrated orbit.

## 5.2 Numerical orbits: Poincaré Plots

In order to verify the analytic calculation and to show what happens when its applicable parameter limits are exceeded, it is helpful to perform a numerical integration of the trapped orbits. The full (non-relativistic) equations of motion for the model potential have been implemented in cylindrical coordinates using a 4th order Runge-Kutta numerical scheme with timestep chosen short enough that the (known) conservation of  $W$  and  $p_{\theta}$  are reproduced for long orbits to no worse than 10 times machine precision. This is observed to require  $\Omega \cdot dt \lesssim 0.05$ . Figures 1 and 2 are examples of orbits so calculated.

Poincaré plots of the energy trajectories for such orbits are obtained by collecting values of  $W_{\parallel}$  and the phase of  $v_r$  (i.e.  $\text{atan2}(v_{\theta}, v_r)$ ) at successive instants when the orbit passes through  $z = 0$  (at which the orbit bounce phase is zero or  $\pi$  and the phase of  $E_n$  is zero for all even  $n$ ). The phase difference,  $\xi$ , thus equals the phase of  $v_r$ . We place a point at each of the corresponding positions in  $\xi, W_{\parallel}$  space. We also, for convenience, start all orbits at  $z = 0$  and with  $v_{\theta} = 0$ ,  $v_r$  positive:  $\xi = 0$ . We abandon as escaped any orbits that acquire positive  $W_{\parallel}$  or pass beyond  $|z| = 20$ . A technical subtlety is that it is most appropriate to use for  $W_{\parallel} = v_z^2/2 - \phi$ , not the value of  $\phi$  at the orbit, but rather the value of  $\phi$  at the *gyrocenter*, which gives significantly smaller oscillatory excursions of  $W_{\parallel}$ . It therefore more effectively suppresses the  $\omega_n + \Omega$  term and expresses the approximate magnetic moment conservation.

Fig. 6(b) shows an example of a Poincaré plot, alongside its analytic energy trajectories 6(a). The agreement is excellent. Orbits are initialized at equally spaced  $W_{\parallel}$  values. Of course, they cannot trace island contours well inside their separatrices where the island does not extend past  $\xi = 0$ . The position and  $W_{\parallel}$ -width of the  $n = 2$  island agree quantitatively very well between (a) and (b). And the  $n = 4$  and  $n = 6$  islands are also readily seen at their expected positions. Between the islands, the Poincaré points trace the open contours. Above

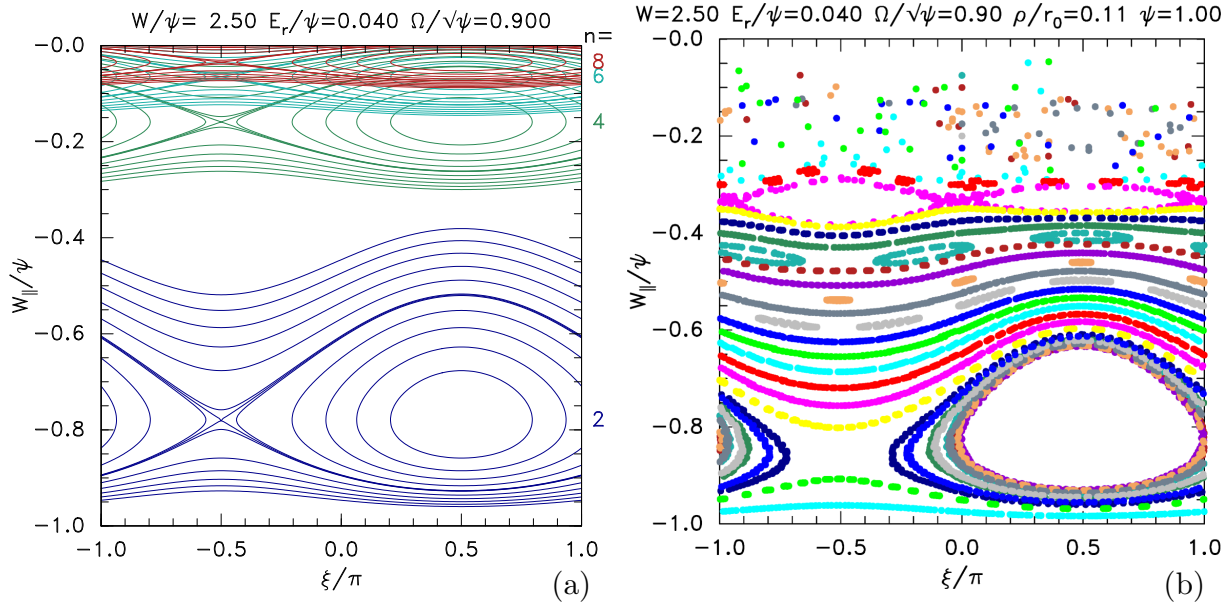


Figure 7: (a) Analytic energy trajectories for different harmonics ( $n$ ), and fixed magnetic field strength and (b) Poincaré plot of the corresponding numerically integrated orbit, for a stronger transverse electric field.

the position of the  $n = 6$  island ( $W_{\parallel}/\psi \geq -0.05$ ) and near its x-point the plot shows rather incoherent scatter of the points. Orbits above this energy are stochastic, and terminate after some tens of bounces by leaving the domain. Again, this agrees well with the analytic observation of overlap between  $n = 6$  and 8, but not between  $n = 4$  and 6 islands.

Fig. 7, by comparison, shows what happens if the amplitude of the perturbing transverse field is increased by a factor of 8, other parameters unchanged. The  $n = 4$  and 6 islands now overlap strongly, and the entire region  $W_{\parallel}/\psi \gtrsim -0.3$  becomes stochastic. Below it, the Poincaré plots show orbits to be permanently trapped. Small island chains with higher mode numbers in phase  $\xi$  become visible. For example the chain of 3 islands at  $W_{\parallel}/\psi \simeq -0.45$ , or of two islands at  $W_{\parallel}/\psi \simeq -0.34$ . These additional chains arise from nonlinearity, and are not represented in the analytic linearized approximation. Still, the overall extent of the  $n = 2$  island is quite well captured by the analytics, which predict that it should remain intact, as it does. If the perturbing  $E_r/\psi$  is increased to 0.1, then overlap and stochasticization of even the  $n = 2$  island begins, as illustrated by Fig. 8. Soon beyond it, by  $E_r/\psi = 0.13$ , essentially the whole of the phase space becomes stochastic.

Fig. 9 shows what happens for a lower magnetic field,  $\Omega/\sqrt{\psi} = 0.6$ . In this case, a field  $E_r/\psi = 0.04$  is sufficient to make the  $n = 2$  island stochastic, but when that happens, there still remain some permanently trapped orbits at energies sufficiently below the resonance value ( $\sim 0.6^2$ ).

In contrast, as shown in Fig. 10, increasing the magnetic field to  $\Omega/\sqrt{\psi} = 1.8$ , removes the  $n = 2$  resonance; and because the higher resonances are weaker, the orbits can sustain higher  $E_r/\psi$  before becoming stochastic. This stabilizing effect is enhanced by the resulting reduction in gyroradius  $\rho$ .

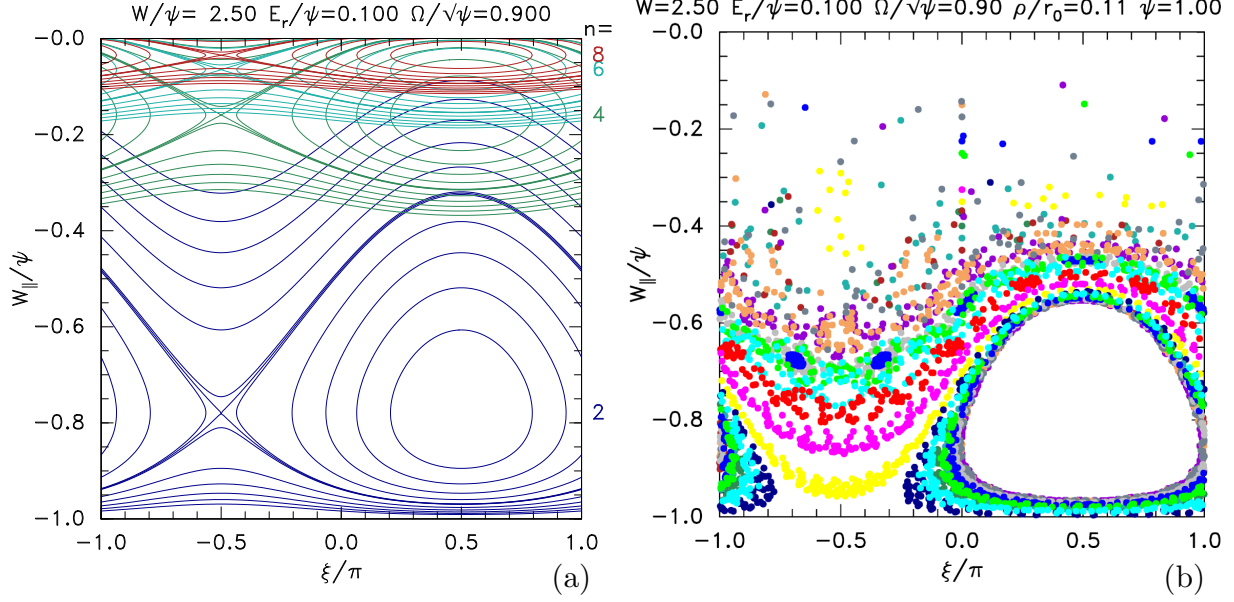


Figure 8: (a) Analytic energy trajectories for different harmonics ( $n$ ), and fixed magnetic field strength and (b) Poincaré plot of the corresponding numerically integrated orbit, for an extremely strong transverse electric field.

## 6 Island widths, overlap, and trapped phase space

In the previous section we have shown that the island overlap criterion successfully predicts which trajectories are stochastic (and hence become untrapped) and which are permanently trapped. We therefore rely on this success and formulate an analytic condition for particles at different locations in phase space to be permanently trapped. We will take those parallel energies  $W_{\parallel}$  to be trapped which lie *below the bottom of the lowest overlapped island* and all others to be subject to detrapping. This criterion describes within typically 10% in  $W_{\parallel}$  what has been observed in the example cases we have shown.

The function  $F_n$ , for fixed  $w$  and  $w_{\parallel R}$ , is stationary at resonance ( $\sqrt{w_{\parallel}} = \sqrt{w_{\parallel R}}$ ), and its derivative in the vicinity of the resonance can be taken from eq. (21) as

$$\begin{aligned} \frac{\partial F_n}{\partial \sqrt{w_{\parallel}}} &= 2\sqrt{w_{\parallel}} \frac{\partial F_n}{\partial w_{\parallel}} \\ &= \frac{n(\sqrt{w_{\parallel}} - \sqrt{w_{\parallel R}})}{\sqrt{2}\sqrt{w + w_{\parallel}}} \left[ \frac{\sqrt{w_{\parallel}} n/2}{(1 - \sqrt{w_{\parallel}})^m} + \frac{\pi}{8} \right]. \end{aligned} \quad (23)$$

Consequently the width of the island separatrix, which occurs at  $\xi = \pi/2$ , is determined by the  $\sqrt{w_{\parallel}}$  value for which  $F_n(w_{\parallel}) - F_n(w_{\parallel} = w_{\parallel R}) \simeq \frac{1}{2}(\sqrt{w_{\parallel}} - \sqrt{w_{\parallel R}})^2 \frac{\partial^2 F_n}{\partial \sqrt{w_{\parallel}}^2}$  is equal to  $E_{r0}/\psi$ . Therefore, regarding the second derivative as constant (adopting just the second-order term

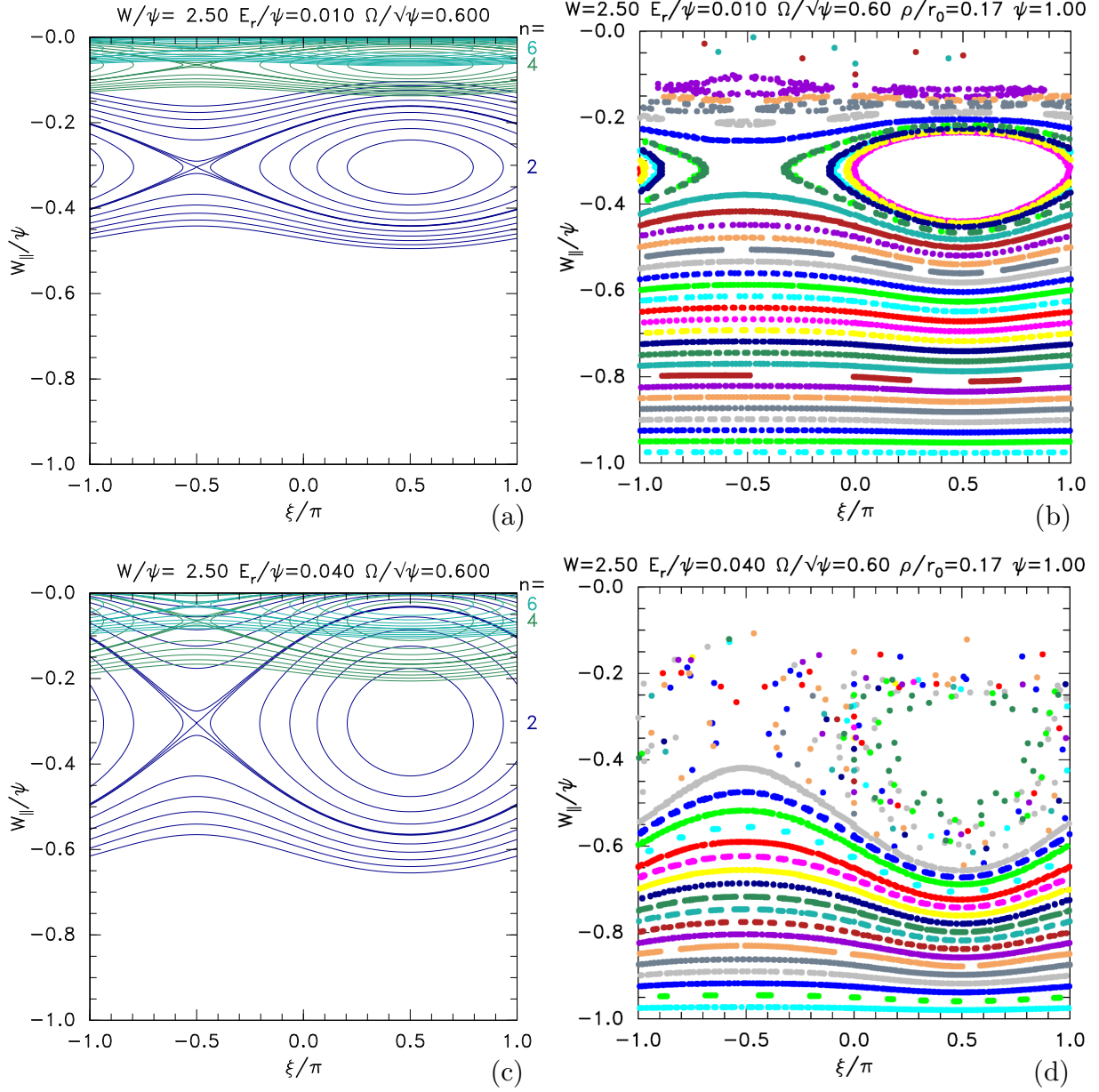


Figure 9: (a),(c) Analytic energy trajectories fixed magnetic field strength and (b),(d) Poincaré plots of the corresponding numerically integrated orbits, for a lower magnetic field, and two perturbation amplitudes.



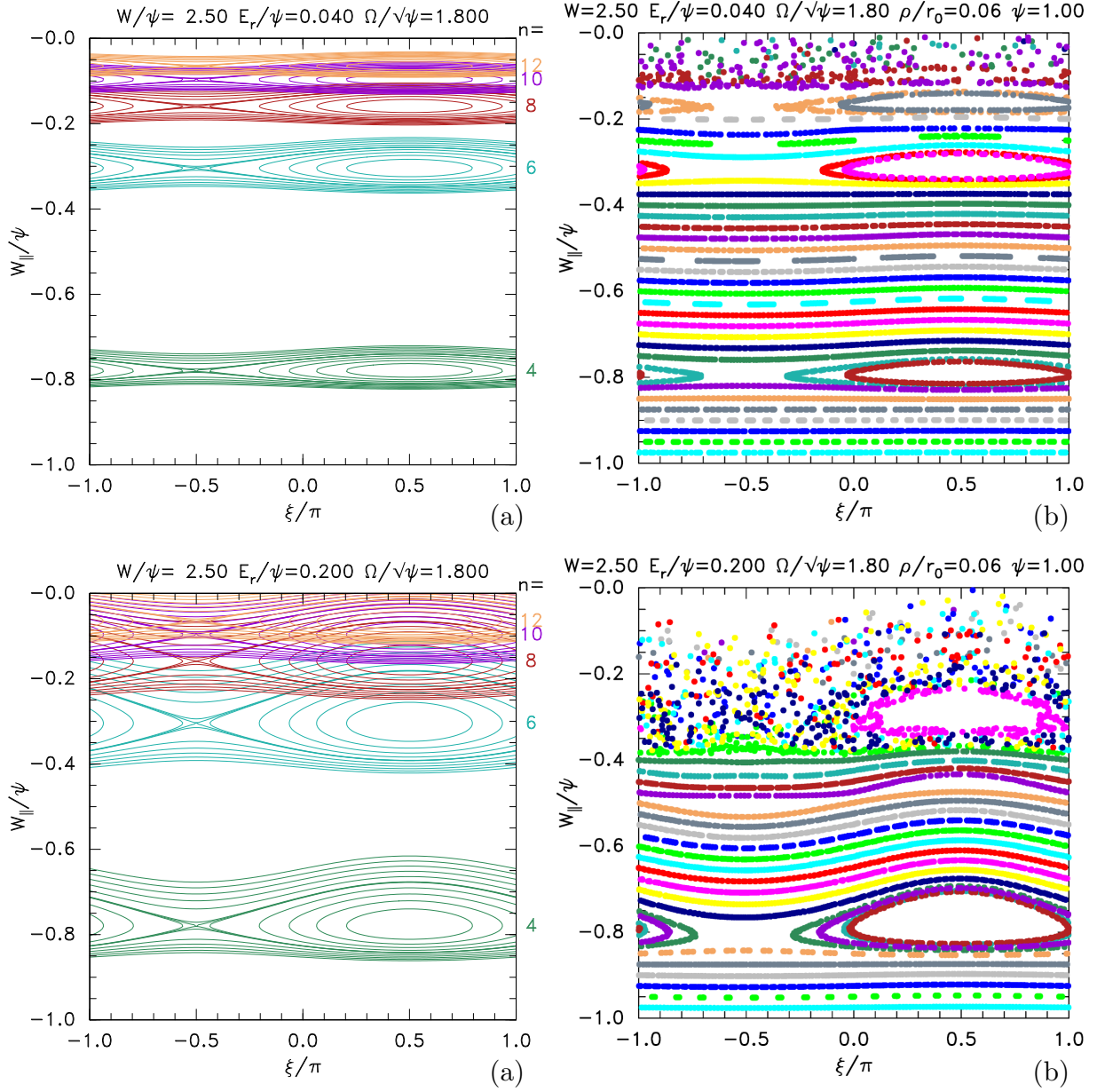


Figure 10: Analytic energy trajectories (a,c), and corresponding Poincaré plots (b,d), for  $\Omega/\sqrt{\psi} = 1.8$ , and  $E_r/\psi = 0.04$  (a,b) or  $0.2$  (c,d).

in a Taylor expansion of  $F_n$ ) we can express the island (half-) width as

$$\begin{aligned}\delta_n &\equiv \sqrt{w_{\parallel}} - \sqrt{w_{\parallel R}} \\ &\simeq \left[ \frac{E_{r0}}{\psi} \frac{2\sqrt{2}}{n} \sqrt{w + w_{\parallel R}} \right]^{1/2} \left[ \frac{\sqrt{w_{\parallel R}} n/2}{(1 - \sqrt{w_{\parallel R}})^m} + \frac{\pi}{8} \right]^{-1/2}.\end{aligned}\quad (24)$$

We write  $w + w_{\parallel R} = w_{\perp}$  ( $\sqrt{2w_{\perp}} = v_{\perp}/\sqrt{\psi}$ ) and recognize that together the parameters  $n$ ,  $E_{r0}v_{\perp}/\psi^{3/2}$ , and  $w_{\parallel R}$  determine  $\delta_n$  as follows.

**Analytic Algorithm** Eq. (14)  $w_{\parallel Rn} = [(n^2/2b^2)^{1/4} + 1 - 2^{1/4}]^{-4}$  enables us to find the energy of the upper and lower island limits of island  $n$  as

$$\begin{aligned}\sqrt{w_{\parallel Rn}} \pm \delta_n &= \\ \sqrt{w_{\parallel Rn}} \pm \left[ \frac{E_{r0}v_{\perp}}{\psi\sqrt{\psi}} \frac{2}{n} \right]^{1/2} \left[ \frac{\sqrt{w_{\parallel Rn}} n/2}{(1 - \sqrt{w_{\parallel Rn}})^m} + \frac{\pi}{8} \right]^{-1/2}.\end{aligned}\quad (25)$$

It is in this equation that one must use the adjustment of  $m$  of eq. (19) for high harmonics. Overlap occurs between the  $n$  and  $n+2$  harmonic islands when  $\sqrt{w_{\parallel Rn}} - \delta_n < \sqrt{w_{\parallel Rn+2}} + \delta_{n+2}$ . Beginning at the lowest value of  $n$  for which a resonance exists (requiring  $w_{\parallel Rn} < 1$ ) determine from evaluation of  $\sqrt{w_{\parallel Rn}} - \delta_n$  and  $\sqrt{w_{\parallel Rn+2}} + \delta_{n+2}$  whether it overlaps with the  $n+2$  island. If so, then it is the *lowest energy overlapped island*; if not, increment  $n$  by 2 and repeat until overlap is found. The resulting  $n$  is the harmonic whose island's lower energy limit is sought, which is

$$W_{\parallel t}/\psi = -w_{\parallel t} = -(\sqrt{w_{\parallel Rn}} + \delta_n)^2. \quad (26)$$

Energies below this approximate bound are predicted trapped, energies above have stochastic orbits and are detrapped.

Figure 11(a) shows the universal contours that result. Where  $W_{\parallel t}/\psi$  is close to zero (light regions), very few orbits are detrapped; while where  $W_{\parallel t}/\psi$  is close to -1 (dark regions) almost all orbits are detrapped. Discontinuities in  $W_{\parallel t}$  occur where  $n$  changes: it starts at 2 at the bottom (right, below  $\Omega/\sqrt{\psi} \simeq 1$ ) and increments through 4,6,... as one moves to larger  $\Omega/\sqrt{\psi}$ . To avoid almost complete detrapping for  $\Omega/\sqrt{\psi} \lesssim 1$ , extremely weak perturbation is required. In contrast, for  $\Omega/\sqrt{\psi} \gtrsim 2$  there is a substantial region of permanently trapped orbits even up to the largest perturbation strength shown.

In Fig. 11(b) are shown vertical profiles through the contours at four values of the perturbation strength, giving  $W_{\parallel t}$  as a function of  $b$ . These lines are each accompanied by points, each of which comes from full numerical orbit integration. A point gives the lowest starting energy that escapes during the first 200 bounces (which might take as many as a million time-steps). We observe that there is very good agreement (even in respect of the discontinuities) between the points and the lines.

A more approximate form of the island widths can be obtained by using  $m = n/2$ , substituting the more approximate frequency fit  $w_{\parallel R} = 4\Omega^2/n^2\psi = 4b^2/n^2$  so that  $\sqrt{w_{Rn}} - \sqrt{w_{Rn+2}} \simeq 4b/n^2$ , and approximating  $(1 - \sqrt{w_{\parallel R}})^{n/2} = (1 - 2b/n)^{n/2} \simeq e^{-b}$ . Then we find  $\delta_n$  is approximately proportional to  $1/\sqrt{n}$  and can be written

$$\delta_n \simeq \left[ \frac{E_{r0}}{\psi} \frac{2\sqrt{2w_{\perp}}}{n} \right]^{1/2} \left[ be^b + \frac{\pi}{8} \right]^{-1/2} \quad (27)$$

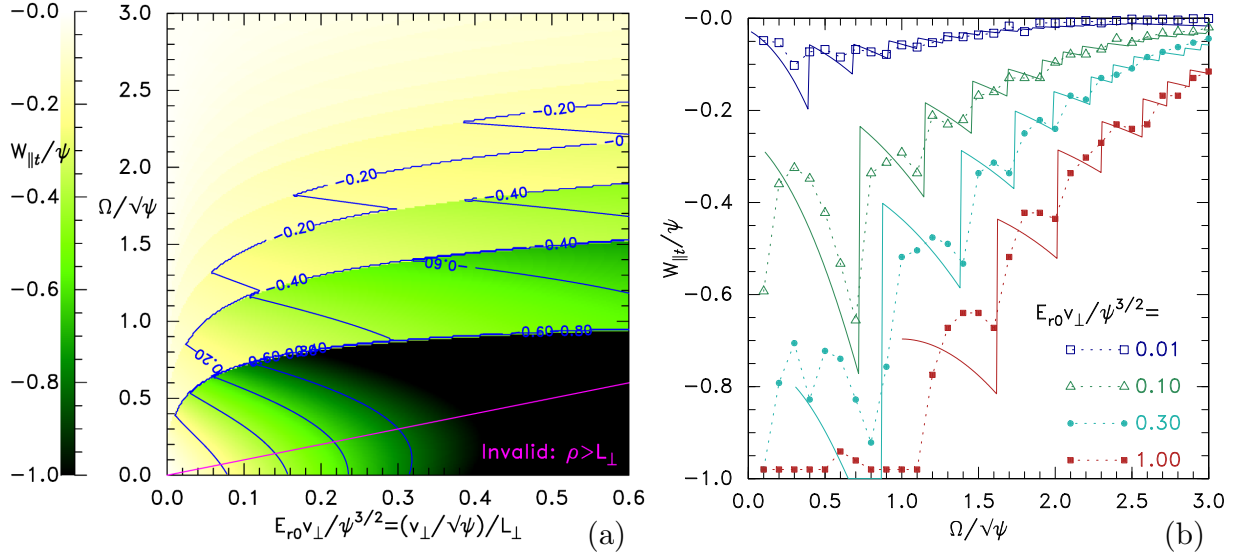


Figure 11: (a) Contours of the energy boundary  $W_{\parallel t}$  between trapped and detrapped orbits as a function of perturbation strength  $E_{r0}v_{\perp}/\psi^{3/2}$  and magnetic field  $\Omega/\sqrt{\psi}$ . (b) The energy boundary  $W_{\parallel t}$  between trapped and detrapped orbits from eq. (26) compared with the lowest detrapped orbits found from numerical orbit integration.

With reference to this approximation, the behavior can readily be understood as follows. Island overlap ( $2\delta_n \gtrsim \sqrt{w_{Rn}} - \sqrt{w_{Rn+2}}$ ) leading to stochastic trajectories occurs if  $\delta_n$  is too large, that is if  $E_{r0}v_{\perp}/\psi$  is too large provided  $b$  ( $= \Omega/\sqrt{\psi}$ ) is not large; or else if  $n$  is too large, making  $\sqrt{w_{Rn}} - \sqrt{w_{Rn+2}}$  too small. The last of these cases (high  $n$  at modest  $E_{r0}$  and  $b$ ) predicts that there is in principle *always* a stochastic region at very small  $w_{\parallel}$ , where the bounce frequency is correspondingly small and the resonant bounce harmonic number large, regardless of the exact  $E_{r0}$  and  $b$  values. Consequently, a steady electron hole of limited transverse extent will always have a stochastic transition between trapped and passing orbits that in practice smooths out any step  $f$ -gradients at the separatrix. Our numerical orbit integration confirms this prediction.

When  $b$  ( $= \Omega/\sqrt{\psi}$ ) is large, the term  $e^b$  makes  $\delta_n$  small, regardless of  $E_{r0}$ , and suppresses overlap. This effect can be considered to arise because when the gyro-period is small compared with the central transit time ( $\tau_t \propto 1/\sqrt{\psi}$ , the duration of the impulse), the Fourier transform of a single impulse has become exponentially small at the cyclotron frequency. The suppression applies at essentially all  $w_{\parallel}$  up to 1, because the impulse width is a rather weak (slowly increasing) function of  $w_{\parallel}$ . Only the exponentially-large- $n$  orbits at exponentially-small- $w_{\parallel}$  will then be stochastic. And the region of stochasticity is limited to very small  $w_{\parallel}$ . High enough magnetic field thus justifies the drift orbit treatment, and eventually imposes no minimum  $L_{\perp}$  requirement for a long-lived hole to exist.

The opposite case  $b \ll 1$  (weak magnetic field) preserves the assumed localization in  $r$  only if the transverse length scale remains greater than the gyro-radius  $E_{r0}/\psi = 1/L_{\perp} \lesssim 1/\rho = \Omega/v_{\perp} = b\sqrt{\psi}/v_{\perp}$  so  $E_{r0}v_{\perp}/\psi^{3/2} \lesssim \Omega/\sqrt{\psi}$ . The valid region of Fig. 11(a) is therefore above the diagonal straight line  $E_{r0}v_{\perp}/\psi^{3/2} = \Omega/\sqrt{\psi}$  drawn in purple. And in Fig. 11(b), the

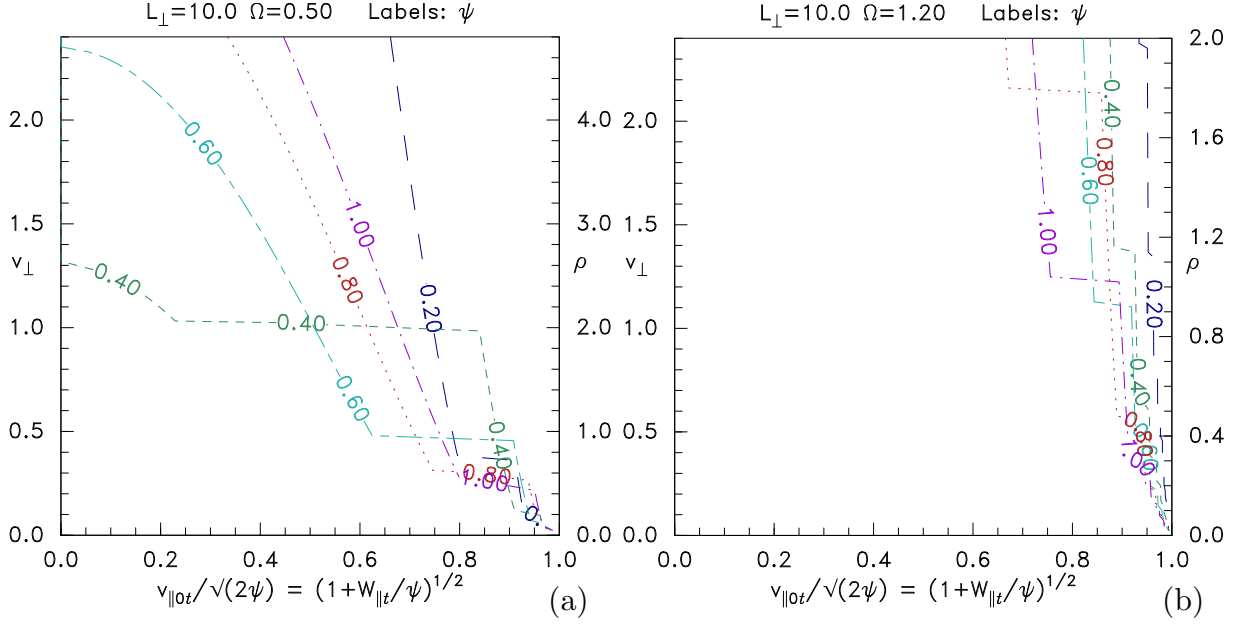


Figure 12: The boundary in velocity-space measured at  $z = 0$  between trapped and untrapped orbits at different  $\psi$ -values: (a) for low magnetic field  $\Omega = 0.5$ , (b) for higher  $\Omega = 1.2$ .

lines are drawn only in the valid region. In the invalid region one can expect the permanent trapping to be poor, and this is confirmed by the points.

A perhaps more intuitive way to portray typical results is as in Fig. 12, where are shown examples of boundaries between trapped and untrapped orbits in velocity-space (based on the island overlap calculation). The important regions of this domain extend to thermal velocities ( $v_{\perp} \gtrsim 1$ , not just  $v_{\perp} \gtrsim \sqrt{\psi}$ ). We need orbits to be permanently trapped for most of the range of possible  $v_{\perp}$  to allow the depression of  $f(v_{\parallel}, v_{\perp})$  to contribute sufficient positive charge to sustain the hole. For smaller  $\psi$  the effective perturbation strength  $\propto v_{\perp}/\sqrt{\psi}L_{\perp}$  becomes stronger for given  $L_{\perp}$ , which makes orbits more easily detrapped. However, the effects of varying resonance condition as  $\psi$  changes are very strong; so the boundaries do not behave monotonically with  $\psi$ . When the  $n = 2$  resonance is avoided, as in Fig. 12(b), the boundary lies at fairly high velocity near  $W_{\parallel} = 0$ . That leads us to expect qualitatively that a distribution  $f(v_{\parallel 0})$  that is approximately flat above  $v_{\parallel 0 t}$ , in the stochastic region, can still sustain an electron hole with these parameters.

In all cases, increasing  $L_{\perp}$  and making the hole more oblate, i.e. closer to one-dimensional reduces the detrapped phase-space area. But unless  $\Omega/\sqrt{\psi} \gtrsim 2$ , holes of large transverse dimension are unstable to transverse perturbations that grow in a few hundred plasma periods and break up the holes into shorter transverse lengths, causing them to collapse. So there is a competition between the requirements of equilibrium and stability.

## 7 Summary

It has been shown that parallel energies of deeply trapped orbits in axisymmetric electron holes have limited excursions in parallel energy, provided the transverse electric field perturbation is weak enough. There is a parallel energy threshold which is a function of perturbation strength and magnetic field, above which the parallel energy trajectory becomes stochastic, and is no longer limited in extent, instead becoming detrapped. Such orbits cannot therefore contribute to the electron deficit needed to sustain the hole. The stochasticity arises when trajectory islands overlap, as has been confirmed by numerical orbit integration. The parallel energy threshold for detrapping has been quantitatively evaluated using the **Analytic Algorithm** as a universal function of the hole parameters. Magnetic fields strong enough that  $\Omega/\sqrt{\psi} \gtrsim 2$  allow a large fraction of the orbits with negative parallel energy to be permanently trapped, even for quite short transverse scale lengths. However, lower magnetic field strengths  $\Omega/\sqrt{\psi} \lesssim 1$  have most of their orbits detrapped unless the transverse scale length is rather large. Although fully self-consistent hole equilibria have not yet been calculated, the present results appear to give an explanation based upon equilibrium trapping constraints for the observation that holes with lower magnetic field and lower peak potential generally must have greater transverse extent than those with greater field or greater potential. Future work will aim to use the quantitative results of this trapped-phase-space calculation, illustrated in Figs. 11 and 12, to explore when fully self-consistent 2D holes can exist and what their forms are likely to be.

## Appendix: Mathematical Function Details

The integrated expressions for  $F_n$  are as follows

$$F_n = \frac{n^2}{2\sqrt{2}}g_m + \frac{n\pi}{16\sqrt{2}}g_0, \quad (28)$$

with

$$g_0 = \int \frac{(\sqrt{w_{\parallel}} - \sqrt{w_{\parallel R}})dw_{\parallel}}{\sqrt{w + w_{\parallel}}\sqrt{w_{\parallel}}}; \quad (29)$$

$$g_m = \int \frac{(\sqrt{w_{\parallel}} - \sqrt{w_{\parallel R}})dw_{\parallel}}{\sqrt{w + w_{\parallel}}(1 - \sqrt{w_{\parallel}})^m}. \quad (30)$$

The first function is easy:  $g_0 = 2[\sqrt{w + w_{\parallel}} - w\sqrt{w_{\parallel R}} \ln(\sqrt{w + w_{\parallel}} + \sqrt{w_{\parallel}})]$ . To evaluate  $g_m$ , define the integrals

$$I_m(a, x) = \int \frac{dx}{\sqrt{a + x^2}(1 - x)^m}, \quad (31)$$

$$J_m(a, x) = \int \frac{x dx}{\sqrt{a + x^2}(1 - x)^m}; \quad (32)$$

then, since  $x^2 = (x - 1)x + x$ , it is easy to show that

$$g_m = 2[(1 - \sqrt{w_{\parallel R}})J_m(w, \sqrt{w_{\parallel}}) - J_{m-1}(w, \sqrt{w_{\parallel}})]. \quad (33)$$

The  $J_m$  and  $I_m$  are related by

$$J_m(a, x) = \int \frac{(x-1) + 1}{\sqrt{a+x^2}(1-x)^m} dx = I_m - I_{m-1}. \quad (34)$$

Also  $J_m$  can be integrated by parts as

$$\begin{aligned} J_m &= \frac{\sqrt{a+x^2}}{(1-x)^m} - m \int \frac{(1-x)^2 - 2(1-x) + 1 + a}{\sqrt{a+x^2}(1-x)^{m+1}} dx \\ &= \frac{\sqrt{a+x^2}}{(1-x)^m} - mI_{m-1} + 2mI_m - m(1+a)I_{m+1}. \end{aligned} \quad (35)$$

Eliminating  $J_m$  between (34) and (35), and gathering terms we obtain the following recursion relation:

$$I_{m+1} = \left[ \frac{\sqrt{a+x^2}}{(1-x)^m} + (2m-1)I_m - (m-1)I_{m-1} \right] \frac{1}{m(a+1)}. \quad (36)$$

Given  $J_0 = \sqrt{a+x^2}$ , and the initial values of the recursion:  $I_0 = \ln(\sqrt{a+x^2} + x)$ , and  $I_1 = [\ln(\sqrt{a+1}\sqrt{a+x^2} + a+x) - \ln(1-x)]/\sqrt{a+x^2}$  we can efficiently obtain by iteration  $I_m$  and  $J_m$  for  $m$  as high as required. This iterative scheme has been implemented and verified, and is used to give the island plots in this paper, which use simply  $m = n/2$ .

## Acknowledgements

I am grateful for useful discussions about transverse structure of electron holes with Ivan Vasko. The codes that were used to do the calculations and create the figures in this article are publically available as doi:10.5281/zenodo.3746740 at <https://zenodo.org/record/3746740> or at <https://github.com/ihutch/AxisymOrbits>. This work was partially funded by NASA grant NNX16AG82G.

## References

- [1] V A Turikov. Electron Phase Space Holes as Localized BGK Solutions. *Physica Scripta*, 30(1):73–77, 1984. URL <http://stacks.iop.org/1402-4896/30/i=1/a=015?key=crossref.1b1e6d048697d81400e82c31ceb2e9bc>.
- [2] Hans Schamel. Electrostatic Phase Space Structures in Theory and Experiment. *Physics Reports*, 140(3):161–191, 1986.
- [3] B Eliasson and P K Shukla. Formation and dynamics of coherent structures involving phase-space vortices in plasmas. *Physics Reports*, 422(6):225–290, jan 2006. URL <http://linkinghub.elsevier.com/retrieve/pii/S037015730500390X>.
- [4] I H Hutchinson. Electron holes in phase space: What they are and why they matter. *Physics of Plasmas*, 24(5):055601, may 2017. URL <http://aip.scitation.org/doi/10.1063/1.4976854>.

- [5] R L Morse and C W Nielson. One-, two-, and three-dimensional numerical simulation of two-Beam plasmas. *Physical Review Letters*, 23(19):1087–1090, 1969.
- [6] H L Berk, C E Nielsen, and K V Roberts. Phase Space Hydrodynamics of Equivalent Nonlinear Systems: Experimental and Computational Observations. *Physics of Fluids*, 13(4):980, 1970. URL <http://scitation.aip.org/content/aip/journal/pof1/13/4/10.1063/1.1693039>.
- [7] Y Omura, H Matsumoto, T Miyake, and H Kojima. Electron beam instabilities as generation mechanism of electrostatic solitary waves in the magnetotail. *Journal of Geophysical Research*, 101(A2):2685, 1996. URL <http://adsabs.harvard.edu/abs/1996JGR...101.2685O>.
- [8] T Miyake, Y Omura, H Matsumoto, and H Kojima. Two-dimensional computer simulations of electrostatic solitary waves observed by Geotail spacecraft. *Journal of Geophysical Research*, 103(A6):11841, 1998. URL <http://doi.wiley.com/10.1029/98JA00760>.
- [9] H Matsumoto, H Kojima, T Miyake, Y Omura, M Okada, I Nagano, and M Tsutsui. Electrostatic solitary waves (ESW) in the magnetotail: BEN wave forms observed by GEOTAIL. *Geophysical Research Letters*, 21(25):2915–2918, dec 1994. URL <http://doi.wiley.com/10.1029/94GL01284>.
- [10] R E Ergun, C W Carlson, J P McFadden, F S Mozer, L Muschietti, I Roth, and R J Strangeway. Debye-Scale Plasma Structures Associated with Magnetic-Field-Aligned Electric Fields. *Physical Review Letters*, 81(4):826–829, jul 1998. URL <http://link.aps.org/doi/10.1103/PhysRevLett.81.826>.
- [11] S D Bale, P J Kellogg, D E Larsen, R P Lin, K Goetz, and R P Lepping. Bipolar electrostatic structures in the shock transition region: Evidence of electron phase space holes. *Geophysical Research Letters*, 25(15):2929–2932, aug 1998. URL <http://doi.wiley.com/10.1029/98GL02111>.
- [12] A Mangeney, C Salem, C Lacombe, J.-L. Bougeret, C Perche, R Manning, P J Kellogg, K Goetz, S J Monson, and J.-M. Bosqued. WIND observations of coherent electrostatic waves in the solar wind. *Annales Geophysicae*, 17(3):307–320, 1999. URL <http://www.ann-geophys.net/17/307/1999/>.
- [13] J S Pickett, L.-J. Chen, R L Mutel, I W Christopher, O Santolk, G S Lakhina, S V Singh, R V Reddy, D A Gurnett, B T Tsurutani, E Lucek, and B Lavraud. Furthering our understanding of electrostatic solitary waves through Cluster multispacecraft observations and theory. *Advances in Space Research*, 41(10):1666–1676, jan 2008.
- [14] L Andersson, R E Ergun, J Tao, A Roux, O Lecontel, V Angelopoulos, J Bonnell, J P McFadden, D E Larson, S Eriksson, T Johansson, C M Cully, D N Newman, M V Goldman, K H Glassmeier, and W Baumjohann. New features of electron phase space holes observed by the THEMIS mission. *Physical Review Letters*, 102(22):225004, 2009.

- [15] L B Wilson, C A Cattell, P J Kellogg, K Goetz, K Kersten, J C Kasper, A Szabo, and M Wilber. Large-amplitude electrostatic waves observed at a supercritical interplanetary shock. *Journal of Geophysical Research: Space Physics*, 115(12):A12104, dec 2010. URL <http://doi.wiley.com/10.1029/2010JA015332>.
- [16] David M Malaspina, David L Newman, Lynn B Willson, Keith Goetz, Paul J Kellogg, and Kris Kerstin. Electrostatic solitary waves in the solar wind: Evidence for instability at solar wind current sheets. *Journal of Geophysical Research: Space Physics*, 118(2): 591–599, 2013.
- [17] D M Malaspina, L Andersson, R E Ergun, J R Wygant, J W Bonnell, C Kletzing, G D Reeves, R M Skoug, and B A Larsen. Nonlinear electric field structures in the inner magnetosphere. *Geophysical Research Letters*, 41:5693–5701, 2014.
- [18] I Y Vasko, O V Agapitov, F Mozer, A V Artemyev, and D Jovanovic. Magnetic field depression within electron holes. *Geophysical Research Letters*, 42(7):2123–2129, 2015.
- [19] F S Mozer, O A Agapitov, A Artemyev, J L Burch, R E Ergun, B L Giles, D Mourenas, R B Torbert, T D Phan, and I Vasko. Magnetospheric Multiscale Satellite Observations of Parallel Electron Acceleration in Magnetic Field Reconnection by Fermi Reflection from Time Domain Structures. *Physical Review Letters*, 116(14):4–8, 2016.
- [20] Ian H Hutchinson and David M Malaspina. Prediction and Observation of Electron Instabilities and Phase Space Holes Concentrated in the Lunar Plasma Wake. *Geophysical Research Letters*, 45:3838–3845, 2018. URL <https://agupubs.onlinelibrary.wiley.com/doi/abs/10.1029/2017GL076880?af=R>.
- [21] F. S. Mozer, O. V. Agapitov, B. Giles, and I. Vasko. Direct Observation of Electron Distributions inside Millisecond Duration Electron Holes. *Physical Review Letters*, 121(13):135102, 2018. URL <https://doi.org/10.1103/PhysRevLett.121.135102>.
- [22] I B Bernstein, J M Greene, and M D Kruskal. Exact nonlinear plasma oscillations. *Physical Review*, 108(4):546–550, 1957. URL <http://journals.aps.org/pr/abstract/10.1103/PhysRev.108.546>.
- [23] J R Franz, P M Kintner, C E Seyler, J S Pickett, and J D Scudder. On the perpendicular scale of electron phase-space holes. *Geophysical Research Letters*, 27(2):169–172, 2000.
- [24] I. Y. Vasko, O. V. Agapitov, F. S. Mozer, A. V. Artemyev, J. F. Drake, and I. V. Kuzichev. Electron holes in the outer radiation belt: Characteristics and their role in electron energization. *Journal of Geophysical Research: Space Physics*, 122(1):120–135, 2017.
- [25] J. C. Holmes, R. E. Ergun, D. L. Newman, N. Ahmadi, L. Andersson, O. Le Contel, R. B. Torbert, B. L. Giles, R. J. Strangeway, and J. L. Burch. Electron Phase-Space Holes in Three Dimensions: Multispacecraft Observations by Magnetospheric Multi-scale. *Journal of Geophysical Research: Space Physics*, 123(12):9963–9978, 2018.



- [26] Y. Tong, I. Vasko, F. S. Mozer, S. D. Bale, I. Roth, A. V. Artemyev, R. Ergun, B. Giles, P. A. Lindqvist, C. T. Russell, R. Strangeway, and R. B. Torbert. Simultaneous Multispacecraft Probing of Electron Phase Space Holes. *Geophysical Research Letters*, 45(21):11,513–11,519, 2018.
- [27] F Mottez, S Perraut, A Roux, and P Louarn. Coherent structures in the magnetotail triggered by counterstreaming electron beams. *Journal of Geophysical Research*, 102(A6):11399, 1997. URL <http://doi.wiley.com/10.1029/97JA00385>.
- [28] M V Goldman, M M Oppenheim, and D L Newman. Nonlinear two-stream instabilities as an explanation for auroral bipolar wave structures. *Geophysical Research Letters*, 26(13):1821–1824, jul 1999. URL <http://doi.wiley.com/10.1029/1999GL900435>.
- [29] M Oppenheim, D L Newman, and M V Goldman. Evolution of Electron Phase-Space Holes in a 2D Magnetized Plasma. *Physical Review Letters*, 83(12):2344–2347, sep 1999. URL <http://link.aps.org/doi/10.1103/PhysRevLett.83.2344>.
- [30] L Muschietti, I Roth, C W Carlson, and R E Ergun. Transverse instability of magnetized electron holes. *Physical Review Letters*, 85(1):94–97, 2000.
- [31] M M Oppenheim, G Vetoulis, D L Newman, and M V Goldman. Evolution of electron phase-space holes in 3D. *Geophysical Research Letters*, 28(9):1891–1894, 2001.
- [32] Nagendra Singh, Sin M Loo, and B Earl Wells. Electron hole structure and its stability depending on plasma magnetization. *Journal of Geophysical Research*, 106(A10):21183–21198, 2001. URL <http://doi.wiley.com/10.1029/2001JA900056>.
- [33] Q M Lu, B Lembege, J B Tao, and S Wang. Perpendicular electric field in two-dimensional electron phase-holes: A parameter study. *Journal of Geophysical Research*, 113(A11):A11219, nov 2008.
- [34] I. H. Hutchinson. Kinematic Mechanism of Plasma Electron Hole Transverse Instability. *Physical Review Letters*, 120(20):205101, 2018. URL <https://doi.org/10.1103/PhysRevLett.120.205101>.
- [35] I H Hutchinson. Transverse instability of electron phase-space holes in multi-dimensional Maxwellian plasmas. *Journal of Plasma Physics*, 84:905840411, 2018. URL <http://arxiv.org/abs/1804.08594>.
- [36] I. H. Hutchinson. Transverse instability magnetic field thresholds of electron phase-space holes. *Physical Review E*, 99:053209, 2019.
- [37] I H Hutchinson. Electron phase-space hole transverse instability at high magnetic field. *Journal of Plasma Physics*, 85(5):905850501, 2019.
- [38] V L Krasovsky, H Matsumoto, and Y Omura. Effect of trapped-particle deficit and structure of localized electrostatic perturbations of different dimensionality. *Journal of Geophysical Research: Space Physics*, 109(A4):A04217, 2004.

- [39] C S Ng and A Bhattacharjee. Bernstein-green-kruskal modes in a three-dimensional plasma. *Physical Review Letters*, 95(24):245004, 2005.
- [40] C S Ng, A Bhattacharjee, and F Skiff. Weakly collisional Landau damping and three-dimensional Bernstein-Greene-Kruskal modes: New results on old problems. *Physics of Plasmas*, 13(5):55903, 2006.
- [41] Li-Jen Chen and G K Parks. BGK electron solitary waves in 3D magnetized plasma. *Geophysical Research Letters*, 29(9):41–45, 2002. URL <http://adsabs.harvard.edu/cgi-bin/nph-data{}?query=bibcode=2002GeoRL..29i..45C{}&link{}type=ABSTRACT{}5Cnpapers3://publication/doi/10.1029/2001GL013385>.
- [42] D Jovanović, P K Shukla, L Stenflo, and F Pegoraro. Nonlinear model for electron phase-space holes in magnetized space plasmas. *Journal of Geophysical Research: Space Physics*, 107(A7):1–6, 2002.
- [43] J G Laframboise and L J Sonmor. Current collection by probes and electrodes in space magnetoplasmas: A review. *Journal of Geophysical Research*, 98(A1):337–357, 1993.
- [44] V. L. Krasovsky, H. Matsumoto, and Y. Omura. Condition for charged particle trapping in a three-dimensional electrostatic potential well in the presence of a magnetic field. *Physica Scripta*, 74(2):227–231, 2006.
- [45] Boris V. Chirikov. A universal instability of many-dimensional oscillator systems. *Physics Reports*, 52(5):263–379, 1979.
- [46] J. D. Meiss. Symplectic maps, variational principles, and transport. *Reviews of Modern Physics*, 64(3):795–848, 1992.
- [47] B. V. Chirikov. Resonance processes in magnetic traps. *The Soviet Journal of Atomic Energy*, 6(6):464–470, 1960.
- [48] H Schamel. Theory of Electron Holes. *Physica Scripta*, 20(3-4):336–342, sep 1979. URL <http://stacks.iop.org/1402-4896/20/i=3-4/a=006?key=crossref.3ff4cf0249a07590ee06c40aee0b5635>.
- [49] I. Y. Vasko, V. V. Krasnoselskikh, F. S. Mozer, and A. V. Artemyev. Scattering by the broadband electrostatic turbulence in the space plasma. *Physics of Plasmas*, 25(7):072903, 2018.